On-water surface synthesis of crystalline two-dimensional polymers assisted by surfactant monolayers

Kejun Liu[1]†, Haoyuan Qi[2]†, Renhao Dong[1]†, Rishi Shivhare[1], Matthew Addicoat[3], Tao Zhang[1], Hafeesudeen Sahabudeen[1], Thomas Heine[1,4], Stefan Mannsfeld[1], Ute Kaiser*[2], Zhikun Zheng*[1], Xinliang Feng*[1]

[1] *Center for Advancing Electronics Dresden (cfaed) & Faculty of Chemistry and Food Chemistry, Technische Universität Dresden, 01062 Dresden, Germany.*

[2] *Central Facility of Electron Microscopy, Electron Microscopy Group of Materials Science, Universität Ulm, 89081 Ulm, Germany*

[3] *School of Science and Technology, Nottingham Trent University, Clifton Lane, NG11 8NS Nottingham, United Kingdom*

[4] *Wilhelm-Ostwald-Institute for Physical and Theoretical Chemistry, Universität Leipzig, 04103 Leipzig, Germany.*

Correspondence to: ute.kaiser@uni-ulm.de; zhikun.zheng@tu-dresden.de; xinliang.feng@tu-dresden.de

†Those authors contribute equally to this work.

Abstract:

Despite rapid progress in recent years, it has remained challenging to prepare crystalline two-dimensional polymers. Here, we report the controlled synthesis of few-layer 2D polyimide crystals on the water surface, through reaction between amine and anhydride monomers, assisted by surfactant monolayers. We obtained 2D polymers with high crystallinity, a thickness of approximately 2 nm, and an average crystal domain size of around 3.5 μm^2. The molecular structure of the materials, their grain boundaries, and their edge structures were characterized using X-ray scattering and transmission electron microscopy techniques, and supported by computations. The formation of crystalline polymers is attributed to the pre-organization of monomers at the water−surfactant interface. Depending on its polar head, the surfactant promoted the arrangement of the monomers — and in turn their polymerization — either horizontally or vertically with respect to the water surface. The latter was observed with a surfactant bearing a carboxylic acid group, which anchored amine monomers vertically through a condensation reaction. In both instances, micrometre-sized 2D polyamide crystals were grown.

Both synthetic and natural polymers play an essential and ubiquitous role in our daily life[1-3], and they typically can be described by a sequence of linearly connecting repeat units via covalent bonds according to the definition proposed by Hermann Staudinger in the early 1920s[4]. There have been numerous impressive attempts to go beyond Staudinger's concept and synthesize sheet-like polymers with long-range order along two orthogonal directions, namely 2D polymers, which can date back to Gee's experiments on interfacial polymerization in 1935[5], Blumstein's cross-linked polymer in interlayer space of montmorillonite clay in 1958[6], and Stupp's bulk polymerization within a self-assembled bilayer in 1993[7]. However, no real structurally-defined 2D polymer has been obtained until the successful discovery of isolation of graphene layer from graphite, a prototype example of 2D polymers from nature[8-10]. The discovery of graphene has also inspired vigorous research efforts devoted to rational synthesis of 2D polymers. For instance, pioneering works on 2D poly(*m*-phenylene) and covalent assemblies of porphyrin and thiophene have been reported via on-surface synthesis under ultra-high vacuum[11-15]. However, the mobility of monomers on the surface is limited and only small domain sizes (generally tens of nanometres) have been obtained. In addition, 2D polymers can also be achieved through a solution exfoliation of van der Waals (vdWs) layer-stacked 2D covalent-organic frameworks[16] or polymer crystals[17-19] synthesized by solvothermal method and/or solid-state polymerization. Despite its success, the exfoliation of defined thin layer structures as well as the precise control over their lateral sizes and thickness remain a challenge. Very recently, free-standing, crystalline, single- or few-layer films of 2D polymers have been developed via the air/water[20-23] and liquid/water[23-25] interfacial synthesis by us and others. Nevertheless, the crystallinity of the resultant 2D polymers remains unsatisfactory with small crystalline domain sizes (typically tens of nanometres), which poses a potential limitation to the development of reliable functions for this emerging class of organic 2D materials.

Here we report a general strategy for the controlled synthesis of few-layer 2D polymer crystals to realize high crystallinity and domain size of several micrometres. Meanwhile, more defined thickness control can also be achieved. We employed surfactant monolayers on the water surface to guide the initial arrangement of rigid and symmetric monomers as well as their 2D polymerization. Few-layer 2D polyimide (**2DPI)** with square lattice was firstly synthesized by condensation reaction of 4,4',4",4'"-(porphyrin-5,10,15,20-tetrayl)tetraaniline (monomer **1**) and isochromeno[4',5',6':6,5,10]anthra[2,1,9-def]isochromene-1,3,8,10-tetrone (monomer **2**) with the assistance of sodium (9Z)-octadec-9-en-1-yl sulfate (sodium oleyl sulfate, SOS). The resulting **2DPI** featured with ~ 2 nm thickness (corresponding to ~5 layers) and an average crystal domain size of ~3.5 μm^2. We further extended this surfactant-assisted on-water surface synthesis strategy to the polycondensation reaction of monomer **1** and 1H,3H-Furo[3,4-f][2]benzofuran-1,3,5,7-tetrone (monomer **3**), providing crystalline few-layer 2D polyamide (**2DPA**) with dual-pore lattice structures. Under the SOS monolayer, **2DPA** adopted a face-on configuration with a crystal domain size of ~ 0.3 μm^2. By unitizing octadecanoic acid (stearic acid, SA) monolayer, we achieved edge-on-oriented **2DPA** with significantly increased domain size (~ 121 μm^2). The molecular structures, grain boundaries and edge structures of the 2D polymers were investigated by grazing-incidence wide-angle X-ray scattering (GIWAXS) and aberration-corrected high-resolution transmission electron microscopy (AC-HRTEM) with the support of theoretical modeling. Our results manifest that the pre-organization of monomers under the surfactant monolayer contributes to the formation of 2D polymer crystals.

Results and discussion

Synthesis of 2DPI on water surface

To synthesize **2DPI**, we prepared a monolayer of SOS (Fig. 1a) on the water surface, and then added monomer **1** (1.5×10^{-7} mol) into the water phase. The adsorption and subsequent

pre-organization of monomer **1** underneath the surfactant monolayer were facilitated by electrostatic interactions and hydrogen bonding. Next, monomer **2** (3.0×10^{-7} mol) was injected into the water phase and then diffused to the pre-organized monomer **1** where 2D polymerization was triggered on the water surface. The polycondensation reaction was left at 20 °C under ambient condition for 7 days, affording the few-layer **2DPI** crystals (Fig. 1b and Supplementary Fig. 1). The formation of imide bonds in **2DPI** was confirmed by the Fourier transform infrared spectroscopy (FTIR) with the appearance of C=O characteristic peak (1695 cm^{-1}), as well as the elimination of N-H stretch ($\nu_{primary\ amino}$, 3350 cm^{-1}) of monomer **1** and the C=O vibration ($\nu_{carboxylic\ dianhydride}$, 1755 cm^{-1}) of monomer **2** (Supplementary Fig. 2). UV-Vis absorption spectrum of **2DPI** exhibited the characteristic Soret (S) band at 437 nm and Q band at 748 nm, which corresponded to the porphyrin structure in **2DPI** (Supplementary Fig. 2)[26].

Structural characterization of 2DPI

For structural characterizations, the **2DPI** film was horizontally transferred onto SiO_2/Si substrates and holey copper TEM grids. After removing the surfactant with chloroform, the film remains stable and homogeneous (Fig. 1c). Atomic force microscopy (AFM) measurement on the SiO_2/Si wafer shows a film thickness of ~ 2 nm, corresponding to ~ 5 layers (Fig. 1d and the inserted height profiles). When transferred onto a holey copper grid, the film freely suspends over the hexagonal mesh with a side length of ~ 25 μm (Supplementary Fig. 3). Bright-field TEM shows that the polymer crystals (dark) are bridged by amorphous areas (bright) in the thin film (Fig. 2a). The areal ratio between the crystalline and amorphous regions is ~ 2.2, which indicates that 69% of the tested area is crystalline. In addition, we deposited **2DPI** film on silicon substrate and carried out chemical exfoliation in dichloromethane via sonication. As shown in Supplementary Fig. 4, after exfoliation the **2DPI** film shows step-like structure at the edge of the crystalline domains. AFM

measurement revealed step heights of 0.4±0.10 and 0.7±0.1 nm within different regions, which can be assigned to the thickness of monolayer and bilayers, respectively.

Selected-area electron diffraction performed on the free-standing **2DPI** film reveals a square unit cell with a = b = 30.0 Å (Fig. 3b), agreeing with the AA-stacked or slipped AA-stacked atomic models of **2DPI** derived by density-functional tight-binding (DFTB) calculation (Fig. 2c, Supplementary Tables 1, 2 and 3, Supplementary Fig. 5). Note that, although the slipped-AA structure is the most energy-favorable stacking mode as it minimizes Coulomb repulsion between the layers, the simulated SAED patterns of slipped-AA-stacked and AA-stacked structures do not differ significantly (Supplementary Fig. 5). We then visualized the molecular structure of **2DPI** by AC-HRTEM (Fig. 2c), showing the square lattice with 30.0 Å spacing. Based on AC-HRTEM image simulation (inset, Fig. 2c), the darkest part corresponds to the pores between the porphyrin units (Supplementary Figs. 6 and 7). To address the crystallinity of **2DPI**, SAED was performed at various positions on 3 mm × 3 mm sized grids (Supplementary Fig. 8). We found that all the diffraction patterns in each selected grain are identical, demonstrating that each domain is a single crystal. The average domain size is ~3.5 μm^2, corresponding to a structurally defined 2D polymer with a molecular weight (MW) of ~5.4×10^8 g mol^{-1} (Supplementary Fig. 8). Meanwhile, we observed slight contrast variation in the bright-field (Fig. 2a) and AC-HRTEM (Fig. 2c) images, which reveals the possible presence of crystal defects (a detailed discussion regarding crystal quality can be seen in the Supplementary Information).

We further characterized the edge structure of the **2DPI** domains. Fig. 2d shows a region where two crystalline domains are bridged by amorphous fragments. By comparing the AC-HRTEM image with its fast Fourier transform (FFT) patterns, we found that the domain edges are parallel to the (100) and (010) planes of **2DPI** (Supplementary Fig. 9). Similar to inorganic 2D materials, such as graphene[27-29] and molybdenum disulphide[30,31], we have

identified two types of grain boundaries, namely, tilt boundary (Fig. 2e) and overlapping boundary (Fig. 2f), formed by domain coalescence (Supplementary Fig. 10).

Effect of surfactant monolayer on the crystallinity of 2DPI and model reaction

To investigate the key role of surfactant in the crystallization of **2DPI**, we carried out control experiments without involving surfactants, from which only amorphous films were obtained (Supplementary Fig. 11). We further explored surfactants with different polar groups, including, sodium;2-dodecylbenzenesulfonate (SDBS) and hexadecyl-trimethyl-ammonium bromide (CTAB).

Among them, SDBS functions similar to SOS, which can guide the self-assembly of monomer **1** via electrostatic interaction, thus leading to the formation of **2DPI** crystals. In contrast, cationic surfactant CTAB only resulted in amorphous films (Supplementary Fig. 12), which can be attributed to the poor ordering of monomers under the surfactant monolayer due to the electrostatic repulsion between monomer **1** in aqueous subphase and positively charged CTAB.

To gain insight into the polymerization mechanism, we characterized the thin films by GIWAXS before and after the addition of monomer **2**. As shown in Fig. 3a (left image), the self-assembly of monomer **1** under SOS monolayer shows in-plane peaks at 0.40, 0.56 and 1.30 $Å^{-1}$, corresponding to a square lattice with $a = b = 15.7$ Å and $\gamma = 90^{o}$, which is further confirmed by SAED and AC-HRTEM investigation (Supplementary Fig. 13). And a diffuse arc at 1.58 $Å^{-1}$ (Fig. 3b, left image) suggests that monomers **1** stack face-to-face with a π-π stacking distance of 4.0 Å. Thus, before 2D polymerization, the self-assembled monomers **1** arrange horizontally (named as pre-**H**) on the water surface. After polymerization and removal of surfactants, **2DPI** thin films show in-plane peaks at 0.20, 0.39 and 0.56 $Å^{-1}$, corresponding to the 010, 020 and 220 Bragg peaks of a square lattice with $a = b = 31.4$ Å and $\gamma = 90^{o}$ (Fig. 3a, right image, Supplementary Fig. 14), which well agrees with DFTB,

AC-HRTEM and SAED results. The out-of-plane stacking distance of 4.0 Å is maintained after polymerization (Fig. 3b, right image). As shown in Fig. 3c, the lattice parameter of pre-**H** is around half of that of **2DPI**, favoring the growth of **2DPI** along the [100] and [010] directions, likely because of the lattice matching between the (100)/(010) planes of pre-**H** ($d_{100,\text{ pre-H}}$ = 15.7 Å) and (200)/(020) planes of **2DPI**.

With evidence of GIWAXS, AC-HRTEM and SAED results, we have confirmed the pre-organization of monomers under the surfactant monolayer and the subsequent imidization reaction forming highly ordered 2D polymers on water surface at ambient conditions. Despite that the realization of imidization reaction in solution generally requires elevated temperature (above 100 °C)[32,33], its reaction rate could be significantly accelerated by on-water synthesis[34-36]. Here, a model reaction based on 5-(4-aminophenyl)-10,15,20-(triphenyl)porphyrin and monomer **2** was carried out on the water surface at room temperature, which readily provided targeted imide compound (Supplementary Fig. 15 and 16). In contrast, the same imidization reaction failed to afford any products in aqueous solution. As illustrated by artificial force induced reaction (AFIR) calculation[37,38], the feasibility of the reaction at ambient conditions originates from the pre-organization of the monomers with self-assembled structures on the water surface (Supplementary Figs. 17 and 18), which accelerates the imidization condensation.

Synthesis of 2DPA on water surface

To demonstrate the generality of our interfacial synthesis approach, we further explored the synthesis of **2DPA** crystals by polymerization of monomers **1** and **3** at SOS-water interface under similar synthesis conditions. As a result, we achieved a crystalline 2D polymer with a dual-pore structure (Fig. 1b, Supplementary Fig. 1) and a thickness of ~ 10 nm (Supplementary Fig. 19). FTIR results confirmed the formation of polyamide with C=O stretch of amide at 1660 cm^{-1} and N-H stretch at 1335 cm^{-1} (Supplementary Fig. 2). UV-Vis

absorption spectrum of **2DPA** also presented the characteristic Soret (S) and Q bands of porphyrin units at 485 nm and 847 nm, respectively (Supplementary Fig. 2). The AFIR calculation for the reaction pathway of polyamide (Supplementary Figs. 20 and 21) also indicates the same conclusion with imidization reaction, i.e., both on-water effect and pre-organization of monomers can accelerate the polymerization rate.

The average crystalline domains of **2DPA** exhibit a width of 0.1- 0.2 μm and a length of up to 2 μm (Supplementary Fig. 22), revealing anisotropic growth rate during polymerization (Fig. 4a). The areal ratio between the crystalline and amorphous region is ~ 1.9, suggesting that 66% polyamide film is crystalline. The edge of crystal domain of **2DPA** is shown in Supplementary Fig. 23 with layer-by-layer stacking morphology. The SAED pattern shows first order reflections at 0.52 nm^{-1} and 0.65 nm^{-1} (Fig. 4b), corresponding to a rectangular unit cell with lattice constants of a = 15.4 Å and b = 19.2 Å, respectively, which agrees with the DFTB calculation (Supplementary Fig. 24, Supplementary Tables 4 and 5). The crystal structure was further confirmed by AC-HRTEM, in which the darkest parts represent the larger pores of **2DPA** (Fig. 4c, Supplementary Fig. 25 and 26). Similar to **2DPI**, monomer **1** in the **2DPA** crystal has face-on orientation and extends horizontally on the water surface. As presented in Fig. 4d, the grain elongates in [100] direction. The higher growth rate along [100] axis has been attributed to the trivial mismatch between the lattice parameters of **2DPA** (a = 15.4 Å) and pre-**H** (15.0 Å), which favours the crystal growth over that in [010] direction[39].

Control of growth orientation of 2DPA on water surface

So far, we have illustrated that the SOS-water interface guided the face-on arrangement of monomer **1** and resulted in 2D polymer growth with layer-stacking direction perpendicular to the water surface. At this point, tuning of the growth direction becomes another appealing objective. To this end, we employed stearic acid (SA) whose carboxyl group can react with

one amine group in monomer **1**, forming a covalent amide bond at the air-water interface (Supplementary Fig. 27). Consequently, monomer **1** could be vertically anchored under the SA monolayer as precursor (namely, pre-**V**). In contrast to pre-**H**(Fig. 3a, left image), GIWAXS measurement of pre-**V** shows an intensive π-π stacking peak along the in-plane direction (Fig. 5a, left image), which is also supported by SAED (Supplementary Fig. 13d and e), demonstrating the edge-on arrangement of monomer **1** which allows for the 2D polymerization along the vertical direction (Fig. 5b and Supplementary Fig. 28). And compared with pre-**H**, the pre-**V** induced by SA could increase the polymerization rate between monomer **1** and monomer **3** as indicated by the rapid decrease of concentration of monomer **1** in the water subphase during the reaction (Supplementary Figs. 29, 30 and 31). As we expected, the GIWAXS pattern (Fig. 5a, right image) has confirmed that, we have successfully tuned the growth direction of **2DPA** layers from horizontal to vertical (**v2DPA**, Supplementary Fig. 32, Supplementary Fig. 33 and Supplementary Table 5). The presence of 001 reflection in SAED pattern (Fig. 4e) and 001 lattice fringes in AC-HRTEM image (Fig. 4f) further confirmed the edge-on configuration of **2DPA** layers. AFM reveals that **v2DPA** has lamellar morphology and a layer step height of ~ 1.8 nm (Supplementary Fig. 19). The crystallinity of **v2DPA** is significantly higher than that of **2DPA**. No amorphous fragments could be identified within **v2DPA** over 3 mm × 3 mm sized grids, and the crystal domain size of **v2DPA** is as large as ~ 121 μm^2 without significant variation of the in-plane crystallographic orientations (Supplementary Fig. 34).

Conclusions and outlook

In conclusion, we have developed a surfactant-assisted on-water surface synthesis strategy to synthesize 2D polymer crystals (**2DPI** and **2DPA**) under ambient conditions. The long-range ordering structures of both **2DPI** and **2DPA** were elucidated by GIWAXS and SAED, respectively. The crystalline structures and grain boundaries were further visualized via AC-

HRTEM with molecular resolution. The surfactant monolayers were found to play a crucial role in facilitating the pre-organization of monomers, thus accelerating the polymerization rate on the water surface. Despite the current success in this on-water surface synthesis of 2D polymers, the remaining challenges are to reduce the amorphous area and prepare monolayer 2D polymers, as well as to increase the single crystalline domans size, which will be of interest for the fabrication of molecular sieving membranes in the future. In addition, it is highly appealing to expand this synthesis strategy to other 2D polymers using various chemical methodologies including reversible and irreversible covalent bonds.

Methods

Synthesis of 2DPI crystal. 20 μL sodium oleyl sulfate (SOS) (1mg mL^{-1} in chloroform) was spread onto the surface of 100 mL Milli-Q water in a 200-mL beaker. The mean molecular area (*mma*) is 24 $Å^2$, which can be calculated by

$$mma = \frac{A_e M_w}{N_A m}$$

where A_e = 25.12 cm^2, is the effective area; M_w = $M_{w,\,sos}$ = 370.5 g mol^{-1}, is the molecular weight of SOS; N_a = 6.02 × 10^{23} mol^{-1} is the Avogadro constant; and m = m_{sos} = 20 μg, is the mass of surfactant. The *mma* of 24 $Å^2$ allows SOS molecules to form a monolayer as proved by π-*A* isotherm curve in Supplementary Fig. 35. The solvent could evaporate for 30 minutes, then monomer **1** (1 mL, 1 mg mL^{-1} in 0.12 M HCl solution) was injected into the water. We waited 30 minutes for the dispersion of monomer **1** in water, and then injected deprotonated PTCDA solution (2 molar equivalent to monomer **1**, 0.64 mL, 1 mg mL^{-1} PTCDA in 0.08 M LiOH aqueous solution) beneath the water surface. After polymerization of 1 week, the formed **2DPI** film was horizontally transferred onto substrates for characterizations.

Synthesis of 2DPA crystal. **2DPA** was prepared at room temperature in a vial with a diameter of 4 cm and a height of 5 cm. 10 mL Milli-Q water was injected into the vial forming a static air-water interface. Then, 3 μL SOS (1 mg mL^{-1} in chloroform) was spread onto the interface (monolayer, *mma* = 25 $Å^2$). The solvent could evaporate for 30 minutes, then monomer **1** (100 μL, 1 mg mL^{-1} in 0.12 M HCl solution) was injected to the water. We waited for 5 minutes for the dispersion of monomer **1** in water, and then added PMDA solution (2 molar equivalents to monomer **1**, 64 μL, 1 mg mL^{-1} PMDA in 0.04 M LiOH aqueous solution) to the subphase. The vial was transferred into a beaker. A small bottle with 1 mL TfOH (trifluoromethanesulfonic acid) was placed beside the vial (CAUTION: TfOH is a fuming acid, highly volatile and pungent. The operation with TfOH must be done in a fuming hood carefully). The beaker was then sealed during the polymerization process and kept for 1 week.

Synthesis of v2DPA crystal. 100 mL Milli-Q water was injected into a beaker forming a static air-water interface. 15 μL stearic acid (SA, 1 mg mL^{-1} in chloroform) was spread onto the interface. The *mma* is 25 $Å^2$ that allows SA molecules to form a monolayer as proved by π-*A* isotherm curve in Supplementary Fig. 35. The solvent could evaporate for 30 minutes, then monomer **1** (1 mL, 1 mg mL^{-1} in 0.12 M HCl solution) was added to the water subphase. We waited for 5 minutes for the dispersion of monomer **1** in water, and then injected PMDA solution (2 molar equivalents to monomer **1**, 0.64 mL, 1 mg mL^{-1} PMDA in 0.04 M LiOH aqueous solution) in water. The reaction was kept at room temperature for 1 week, or at 50 °C for 12 h.

Substrates. Single- and few-layer 2D polymers were deposited onto 300 nm SiO_2/Si substrate for optical microscopy and atomic force microscopy (AFM), on quartz glass for

UV-Vis absorption spectroscopy, on copper foil for infrared spectroscopy (IR), and on copper grids for transmission electron microscopy (TEM) characterizations.

Characterizations. Mass spectrometry analysis was performed on a Bruker Autoflex Speed MALDI TOF MS (Bruker Daltonics, Bremen, Germany) using dithranol as matrix. Optical images were acquired in differential interference mode with AxioScope A1, Zeiss. Atomic force microscopy (AFM) was performed in air on a customized Ntegra Aura/Spectra from NT-MDT (Moscow, Russia) with a SMENA head operated in contact mode. Aberration-corrected high-resolution transmission electron microscopy (AC-HRTEM) imaging and selected-area electron diffraction (SAED) were conducted on an image-side Cs-corrected FEI Titan 80-300 microscope operated at 300 kV. In order to reduce the electron irradiation damage on 2D polymers, the total electron dose for the acquisition of SAED patterns and HRTEM images was limited to 2.0 $e^-/Å^2$ (dose rate: 0.2 $e^-/Å^2 \cdot s$) and 1000 $e^-/Å^2$ (dose rate: 200 $e^-/Å^2 \cdot s$), respectively. UV-Vis absorption spectra were obtained on an UV-Vis-NIR Spectrophotometer Cary 5000 at room temperature. Fourier-transform infrared spectroscopy (FTIR) was performed on Tensor II (Bruker) with an attenuated total reflection (ATR) unit.

Computational method section. Details of the calculations are given in the Supplementary Information.

Data availability statement. The authors declare that the data supporting the findings of this study are available within the Article and its Supplementary Information or from the corresponding author upon reasonable request.

References:

1. Rodenas, T. *et al.* Metal-organic framework nanosheets in polymer composite materials for gas separation. *Nat. Mater.* **14**, 48-55 (2015).

2. Tessler, N., Denton, G. J. & Friend, R. H. Lasing from conjugated-polymer microcavities. *Nature* **382**, 695-697 (1996).

3. Yu, Y., Nakano, M. & Ikeda, T. Photomechanics: directed bending of a polymer film by light. *Nature* **425**, 145 (2003).

4. Staudinger, H. Über Polymerisation. *Ber. Dtsch. Chem. Ges.* **53**, 1073-1085 (1920).

5. Gee, G. Reactions in monolayers of drying oils. Ii. Polymerization of the oxidized forms of the maleic anhydride compound of beta elaeostearin. *Proc. Royal Soc. A.* **153**, 129-141 (1935).

6. Blumstein, A., Herz, J., Sinn, V. & Sadron, C. Sur un procede de polymerisation en couche adsorbee. *Comptes Rendus Acad. Sci.* **246**, 1856-1858 (1958).

7. Stupp, S., Son, S., Lin, H. & Li, L. Synthesis of two-dimensional polymers. *Science* **259**, 59-63 (1993).

8. Novoselov, K. S. *et al.* Electric field effect in atomically thin carbon films. *Science* **306**, 666-669 (2004).

9. Sakamoto, J., van Heijst, J., Lukin, O. & Schlüter, A. D. Two-dimensional polymers: Just a dream of synthetic chemists? *Angew. Chem. Int. Ed.* **48**, 1030-1069 (2009).

10. Chen, L., Hernandez, Y., Feng, X. & Mullen, K. From nanographene and graphene nanoribbons to graphene sheets: chemical synthesis. *Angew. Chem. Int. Ed.* **51**, 7640-7654 (2012).

11. Grill, L. *et al.* Nano-architectures by covalent assembly of molecular building blocks. *Nat. Nanotechnol.* **2**, 687-691 (2007).

12. Bieri, M. *et al.* Porous graphenes: two-dimensional polymer synthesis with atomic precision. *Chem. Commun.* 6919-6921 (2009).

13. Lafferentz, L. *et al.* Controlling on-surface polymerization by hierarchical and substrate-directed growth. *Nat. Chem.* **4,** 215 (2012).

14. Gutzler, R. & Perepichka, D. π-Electron Conjugation in Two Dimensions. *J. Am. Chem. Soc.* **135,** 16585–94 (2013).

15. Cardenas, L. *et al.* Synthesis and electronic structure of a two dimensional -conjugated polythiophene. *Chem. Sci.* **4**, 3263-3268 (2013).

16. Bunck, D. N. & Dichtel, W. R. Bulk synthesis of exfoliated two-dimensional polymers using hydrazone-linked covalent organic frameworks. *J. Am. Chem. Soc.* **135**, 14952-14955 (2013).

17. Kissel, P. *et al.* A two-dimensional polymer prepared by organic synthesis. *Nat. Chem.* **4**, 287 (2012).

18. Kissel, P., Murray, D. J., Wulftange, W. J., Catalano, V. J. & King, B. T. A nanoporous two-dimensional polymer by single-crystal-to-single-crystal photopolymerization. *Nat. Chem.* **6**, 774-778 (2014).

19. Liu, W. *et al.* A two-dimensional conjugated aromatic polymer via C–C coupling reaction. *Nat. Chem.* **9**, 563 (2017).

20. Payamyar, P. *et al.* Synthesis of a Covalent Monolayer Sheet by Photochemical Anthracene Dimerization at the Air/Water Interface and its Mechanical Characterization by AFM Indentation. *Adv. Mater.* **26**, 2052-2058 (2014).

21. Murray, D. J. *et al.* Large Area Synthesis of a Nanoporous Two-Dimensional Polymer at the Air/Water Interface. *J. Am. Chem. Soc.* **137**, 3450-3453 (2015).

22. Müller, V. et al. A Two-Dimensional Polymer Synthesized at the Air/Water Interface. *Angew. Chem. Int. Ed.* **57**, 10584-10588, (2018).

23. Sahabudeen, H. *et al.* Wafer-sized multifunctional polyimine-based two-dimensional conjugated polymers with high mechanical stiffness. *Nat. Commun.* **7**, 13461 (2016).

24. Dey, K. *et al.* Selective Molecular Separation by Interfacially Crystallized Covalent Organic Framework Thin Films. *J. Am. Chem. Soc.* **139**, 13083-13091 (2017).

25. Matsumoto, M. *et al.* Lewis-Acid-Catalyzed Interfacial Polymerization of Covalent Organic Framework Films. *Chem* **4**, 308-317 (2018).

26. Son, H.-J. *et al.* Light-Harvesting and Ultrafast Energy Migration in Porphyrin-Based Metal–Organic Frameworks. *J. Am. Chem. Soc.* **135**, 862-869 (2013).

27. Huang, P. Y. et al. Grains and grain boundaries in single-layer graphene atomic patchwork quilts. *Nature* **469**, 389–392 (2011).

28. Robertson, A. W. et al. Atomic Structure of Interconnected Few-Layer Graphene Domains. *ACS Nano* **5**, 6610-6618 (2011).

29 S. Kurasch, J. Kotakoski, O. Lehtinen, V. Skakalova, J. H. Smet, C. Krill III, A. V. Krasheninnikov, U. Kaiser Atom-by-Atom Observation of Grain Boundary Migration in Graphene, *Nano Lett.* **12**, 3168–3173 (2012)

30. Najmaei, S. et al. Vapour phase growth and grain boundary structure of molybdenum disulphide atomic layers. *Nat. Mater.* **12**, 754–759 (2013).

31. Van Der Zande, A. M. et al. Grains and grain boundaries in highly crystalline monolayer molybdenum disulphide. *Nat. Mater.* **12**, 554–561 (2013).

32. Baumgartner, B., Puchberger, M. & Unterlass, M. M. Towards a general understanding of hydrothermal polymerization of polyimides. *Polym. Chem.* **6**, 5773-5781 (2015).

33. Fang, Q. *et al.* Designed synthesis of large-pore crystalline polyimide covalent organic frameworks. *Nat. Commun.* **5**, 4503,5503 (2014).

34. Jung, Y. & Marcus, R. A. On the nature of organic catalysis "on water". *J. Am. Chem. Soc.* **129**, 5492-5502 (2007).

35. Narayan, S. *et al.* "On water": unique reactivity of organic compounds in aqueous suspension. *Angew. Chem. Int. Ed.* **44**, 3275-3279 (2005).

36. Butler, R. N. & Coyne, A. G. Water: nature's reaction enforcer--comparative effects for organic synthesis "in-water" and "on-water". *Chem. Rev.* **110**, 6302-6337(2010).

37. Maeda, S. *et al.* Implementation and performance of the artificial force induced reaction method in the GRRM17 program. *J. Comput. Chem.* **39**, 233-251 (2018).

38. Maeda, S., Ohno, K. & Morokuma, K. Systematic exploration of the mechanism of chemical reactions: the global reaction route mapping (GRRM) strategy using the ADDF and AFIR methods. *Phys. Chem. Chem. Phys.* **15**, 3683-3701 (2013).

39. Habas, S. E., Lee, H., Radmilovic, V., Somorjai, G. A. & Yang, P. Shaping binary metal nanocrystals through epitaxial seeded growth. *Nat. Mater.* **6**, 692-697 (2007).

Acknowledgments

The authors gratefully acknowledge financial support by ERC Grant on T2DCP and EU Graphene Flagship, COORNET (SPP 1928), CONJUGATION-706082 as well as the German Science Council, Centre of Advancing Electronics Dresden, EXC1056, (cfaed) and OR 349/1. H.Q. and U.K. thank the financial support by the DFG in the framework of the "SALVE" (Sub-Angstrom Low-Voltage Electron Microscopy) project as well the Ministry of

Science, Research and the Arts (MWK) of Baden-Wuerttemberg in the framework of the SALVE project. K. L. thanks the China Scholarship Council (CSC) for the financial support. We acknowledge Petr Formánek for TEM, Markus Löffler for SEM and Josef Michl for the helpful discussions. GIWAXS was carried out at DESY, a members of the Helmholtz Association (HGF), and at Helmholtz-Zentrum Berlin. We would like to thank M. Schwartzkopf for assistance (P03-MINAXS beamline) and Daniel Többens (KMC-2 beamline). We thank HGF and HZB for the allocation of neutron/synchrotron radiation beamtime. The authors have no conflicting financial interests.

Author Contributions

X. F. conceived and designed the experiments. K. L. and R. D. contributed to the synthesis of 2D polymers and model compounds. H. Q. and U. K. performed AC-HRTEM imaging, SAED and corresponding analysis. R. S., K. L. and H. S. conducted GIWAXS. K. L., H. Q., R. D., R. S., M. A. and S. M. analysed diffraction data and proposed the crystal structures. T. Z. performed AFM imaging. K. L. performed OM, SEM, FTIR and UV-Vis measurements. M. A., R. D., and T. H. contributed to the theory calculation and analysis. K. L., R. D. and X. F. proposed the reaction mechanism. K. L., H. Q., R. D., Z. Z. and X. F. co-wrote the manuscript with contributions from all authors.

Author Information

Reprints and permissions information is available at www.nature.com/reprints. The authors declare no competing financial interests. Readers are welcome to comment on the online version of this article at www.nature.com/nature. Correspondence and requests for materials should be addressed X. F. (xinliang.feng@tu-dresden.de), Z.Z. (zhikun.zheng@tu-dresden.de) and U. K. (ute.kaiser@uni-ulm.de).

Competing interests

The authors declare no competing interests.

Figure Captions

Figure 1 | Synthesis protocol of 2D polymers. **a**, Schematic illustration of the synthetic procedure of 2D polymers on water surface assisted by surfactant monolayer. **b**, Reaction scheme illustrating the synthesis of **2DPI** and **2DPA** by condensation reactions with assistance of surfactant monolayers on water surface. **c**, Optical microscope image of **2DPI** film, (0) and (1) represent the uncovered substrate and film, respectively. **d**, AFM image of **2DPI** film, the traces in green and cyan are AFM height profiles at two selected positions showing ~2.0 nm thickness.

Figure 2 | Structural characterization of 2DPI. **a**, Overview of **2DPI** film by bright-field TEM. Dark regions are crystalline. **b**, SAED pattern from the crystalline domain in (**a**). The arrows indicate the 100 and 010 reflections at 0.33 nm^{-1} (i.e., 3 nm). **c**, AC-HRTEM image of **2DPI** (Inset: simulated image of **2DPI** along the [001] projection with the structure model overlaid; blue, red, green and white dots represent carbon, oxygen, nitrogen and hydrogen atoms, respectively). **d**, AC-HRTEM image of two crystalline domains which are bridged by amorphous fragments. The domain edges are indicated by the red dotted lines. **e**, AC-HRTEM image of a tilt grain boundary. The red and blue dots highlight the positions of porphyrin core of monomer **1** in two neighbored domains, respectively. **f**, AC-HRTEM image of an overlapping grain boundary exhibiting Moiré fringes.

Figure 3 | GIWAXS analysis of transition from pre-H to 2DPI. **a**, in-plane (near $Q_z = 0$) and **b**, out-of-plane (near $Q_{xy} = 0$) diffraction patterns demonstrating the transition from pre-**H** (i.e., monomer **1** self-assembly under SOS monolayer) to **2DPI**. **c**, Schematic of the pre-**H**-to-**2DPI** transition.

Figure 4 | Structural characterization of 2DPA. **a**, Overview of **2DPA** film by bright-field TEM. Dark regions are crystalline. **b**, SAED pattern from the crystalline domain in (**a**). The

100 and 010 reflections are at 0.65 nm^{-1} and 0.52 nm^{-1}, respectively. **c**, AC-HRTEM image of **2DPA** (Inset: simulated image of **2DPA** along the [001] projection with the structure model overlaid; blue, red, green and white dots represent carbon, oxygen, nitrogen and hydrogen atoms, respectively). **d**, AC-HRTEM image of **2DPA** grain edge, which is highlighted by the red dotted line. **e**, SAED pattern of **v2DPA**. The measured 120 and 001 reflections are at 1.29 nm^{-1} and 1.05 nm^{-1} with an angle of 80°. **f**, AC-HRTEM image of **v2DPA** showing the 001 lattice fringes.

Figure 5 | GIWAXS analysis of transition from pre-V to v2DPA. **a**, GIWAXS pattern showing the transition from pre-**V** (i.e., monomer **1** self-assembly under SA monolayer) to **v2DPA**. The white arrow marks the π-π stacking peak. **b**, Schematic of the pre-**V**-to- **v2DPA** transition.

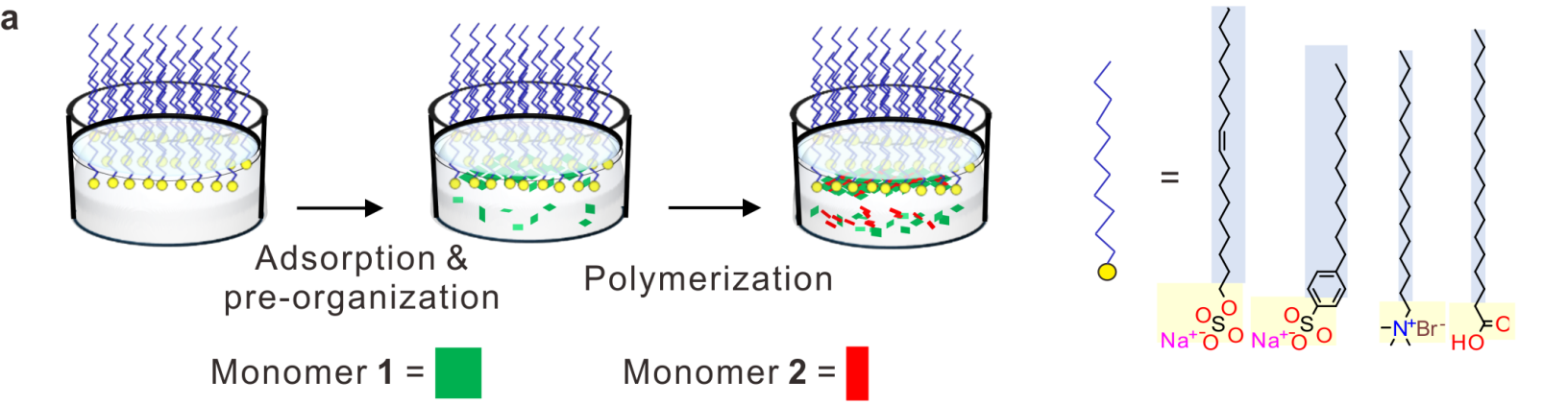
a
Adsorption &
pre-organization
Polymerization
Monomer 1 =
Monomer 2 =
=
Na+ O S O O
Na+ O S O O
N+ Br-
HO C

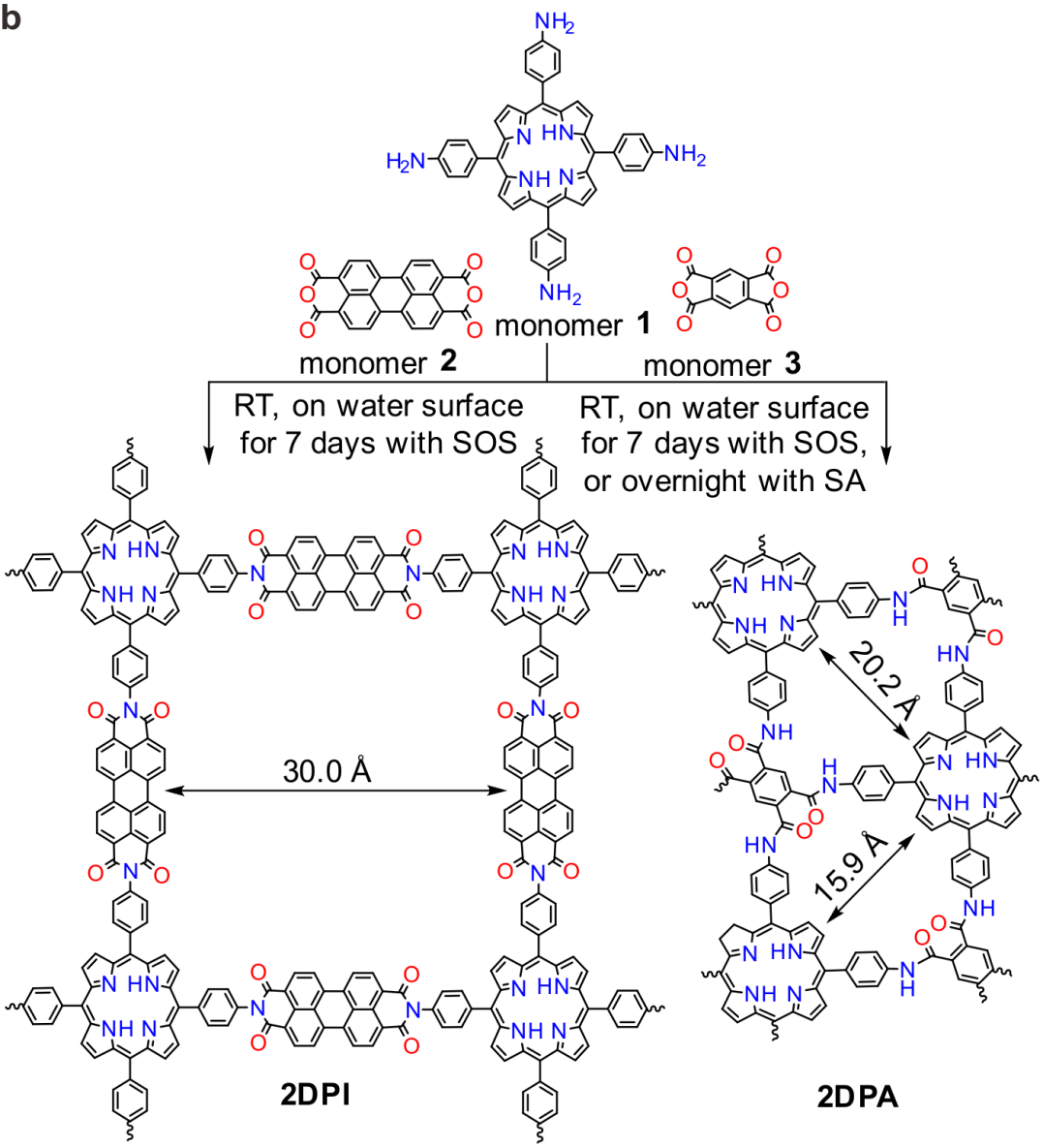
b
NH2
H2N
NH2
NH2
monomer 1
monomer 2
monomer 3
RT, on water surface
for 7 days with SOS
RT, on water surface
for 7 days with SOS,
or overnight with SA
30.0 Å
2DPI
20.2 Å
15.9 Å
2DPA

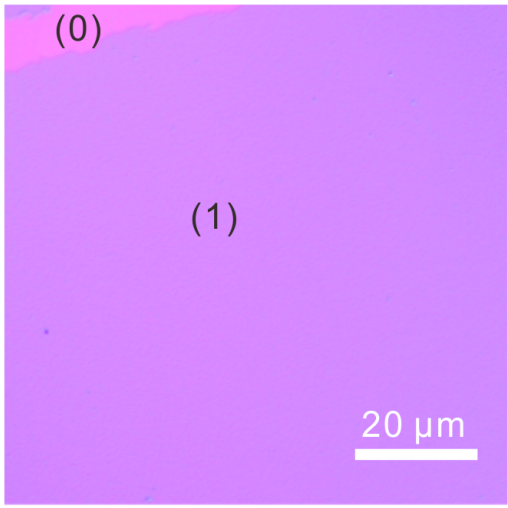
c
(0)
(1)
20 μm

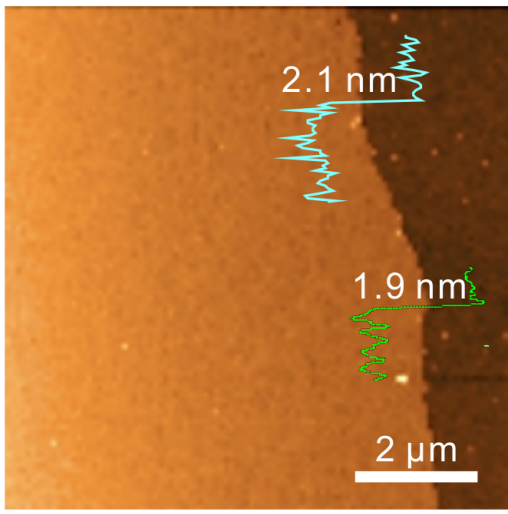
d
2.1 nm
1.9 nm
2 μm

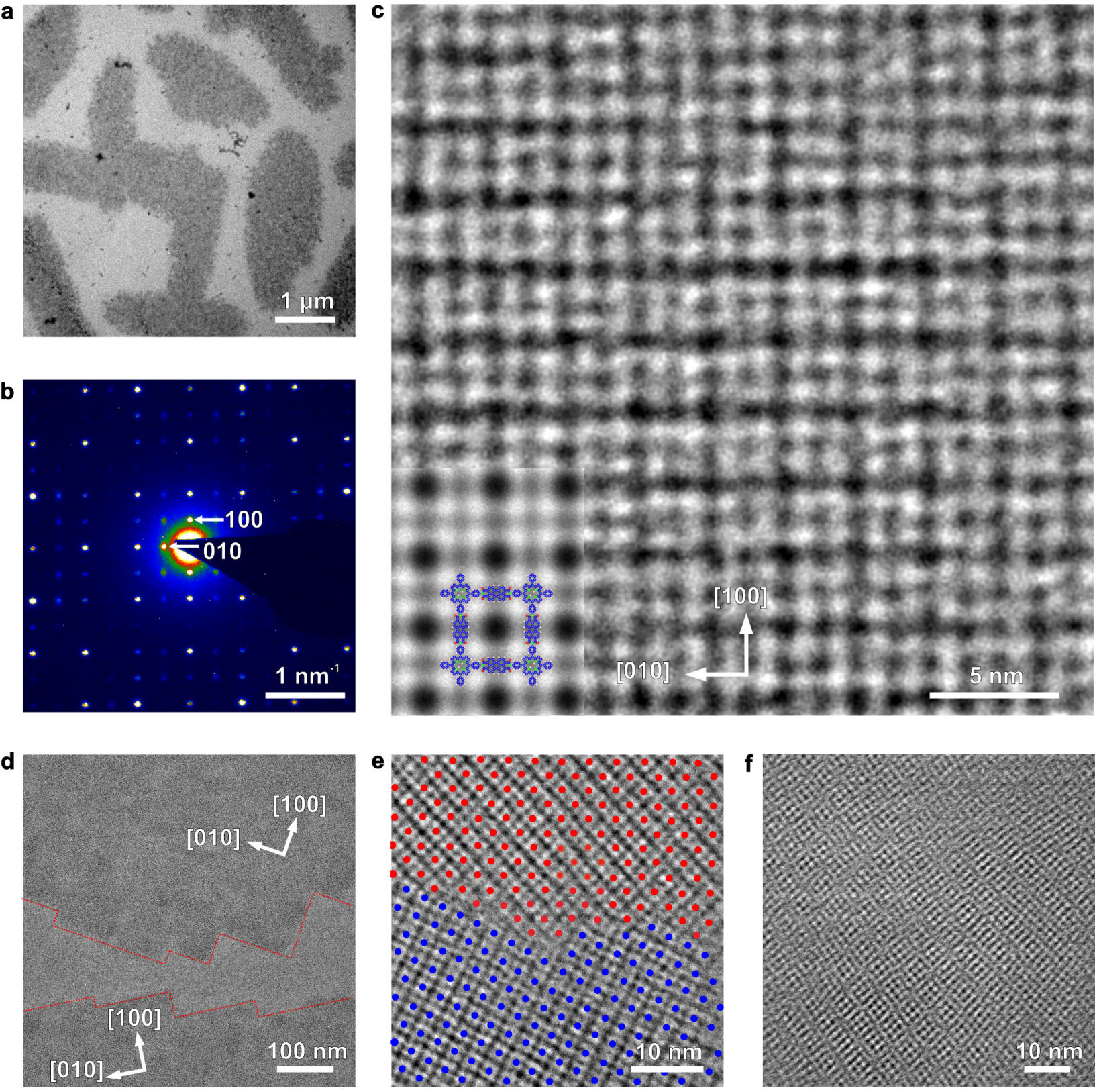
a
1 μm
b
100
010
1 nm-1
c
[100]
[010]
5 nm
d
[100]
[010]
[100]
[010]
100 nm
e
10 nm
f
10 nm

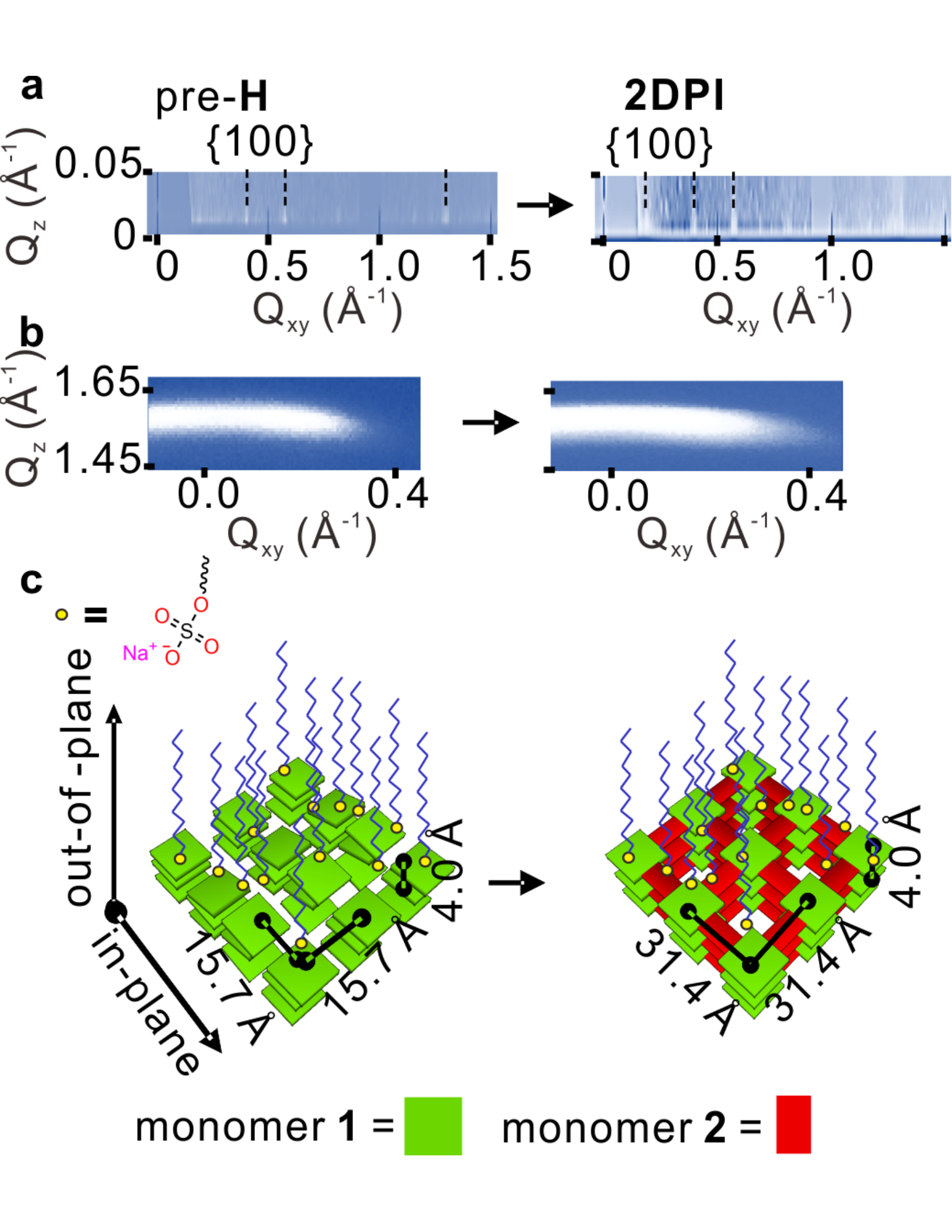
a
pre-H
{100}
2DPI
{100}
0.05
0
Q_z (Å^{-1})
0
0.5
1.0
1.5
Q_{xy} (Å^{-1})
b
1.65
1.45
Q_z (Å^{-1})
0.0
0.4
Q_{xy} (Å^{-1})
c
=
Na^+
out-of-plane
in-plane
15.7 Å
15.7 Å
4.0 Å
31.4 Å
31.4 Å
4.0 Å
monomer 1 =
monomer 2 =

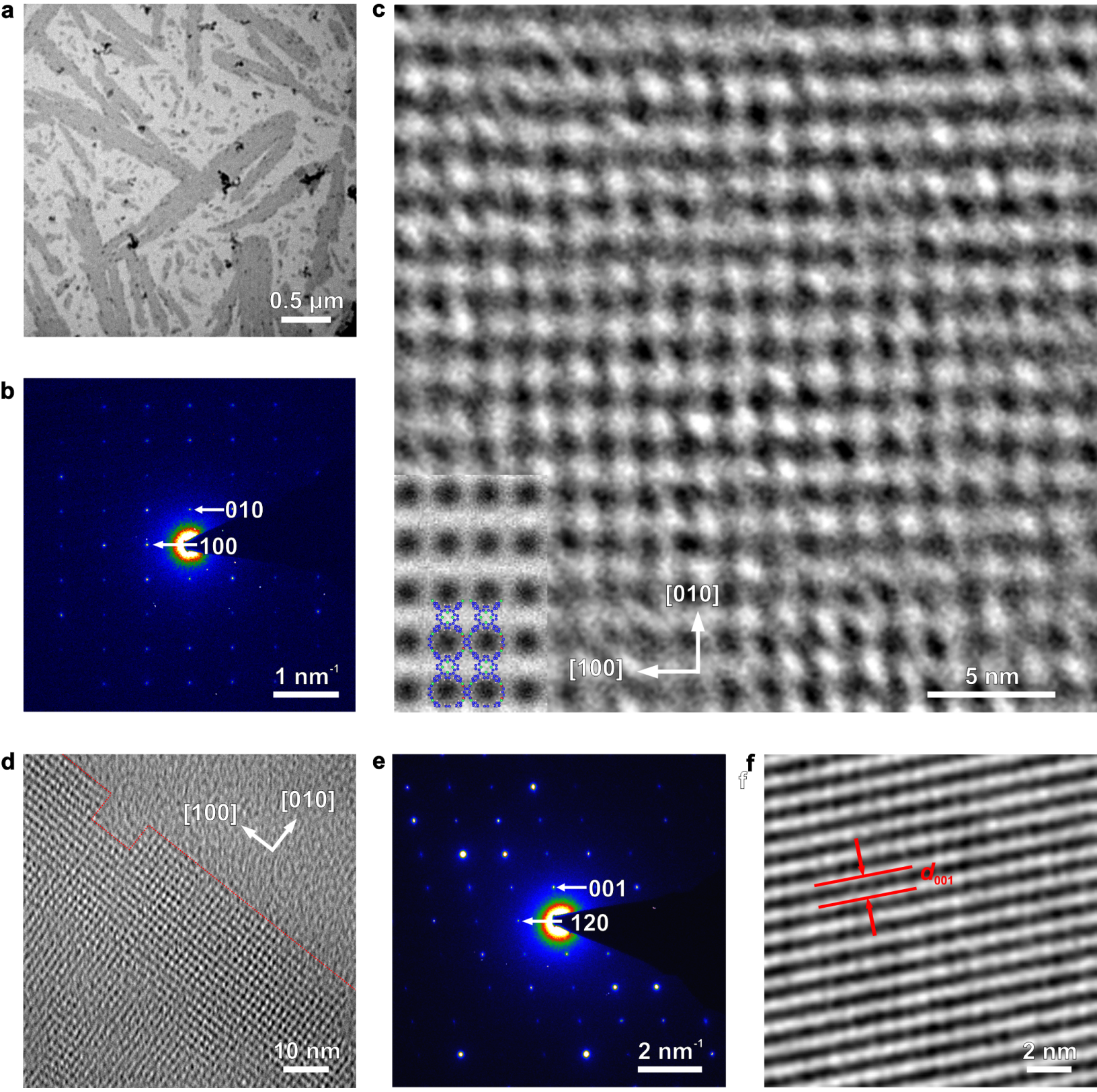
a
0.5 μm
b
010
100
1 nm-1
c
[010]
[100]
5 nm
d
[100]
[010]
10 nm
e
001
120
2 nm-1
f
d001
2 nm

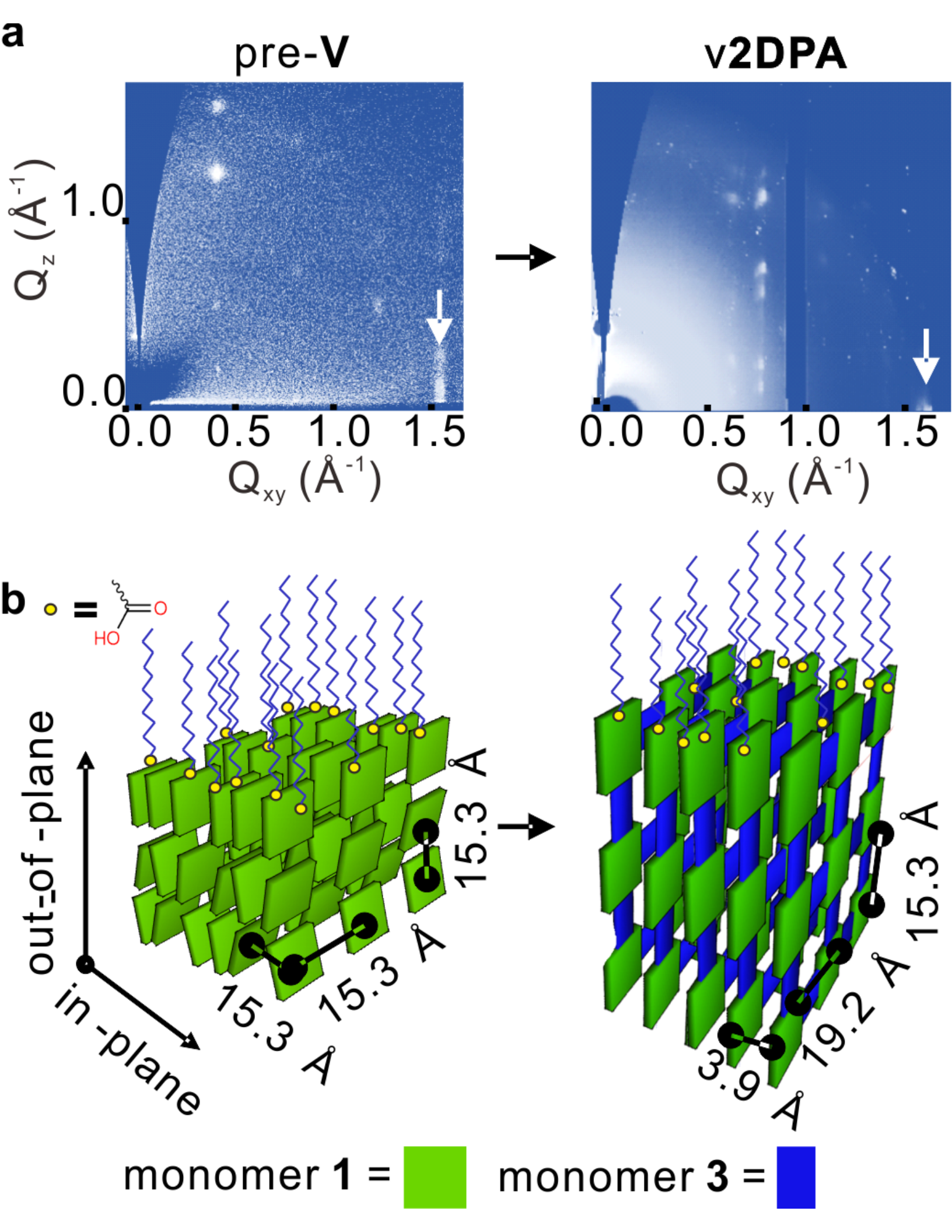
a
pre-V
v2DPA
Q_z (Å^-1)
1.0
0.0
0.0 0.5 1.0 1.5
Q_xy (Å^-1)
0.0 0.5 1.0 1.5
Q_xy (Å^-1)
b
HO
O
out-of-plane
in-plane
15.3 Å
15.3 Å
15.3 Å
15.3 Å
19.2 Å
3.9 Å
monomer 1 =
monomer 3 =

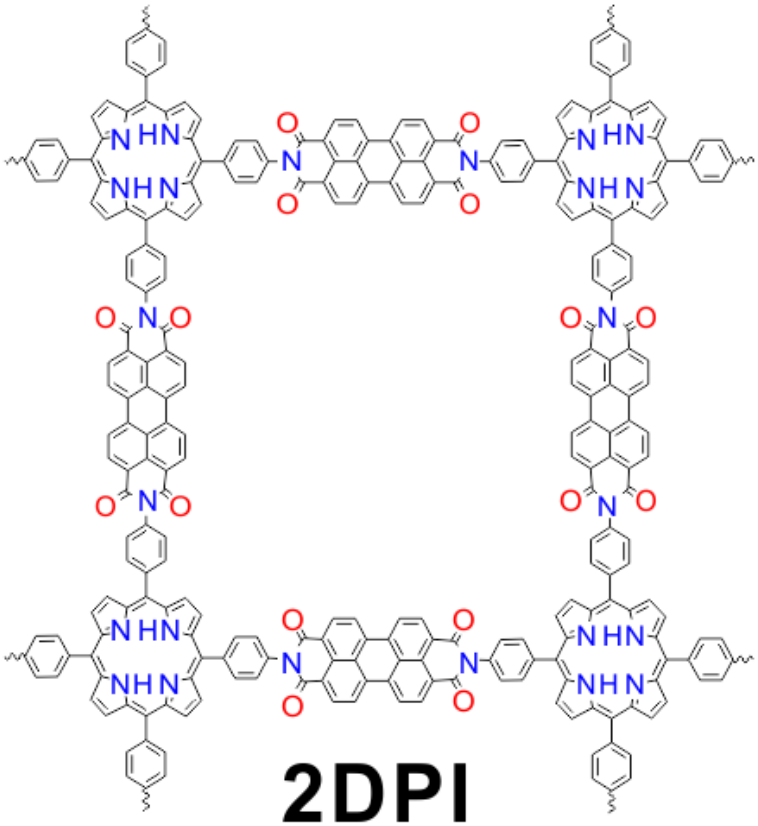
2DPI

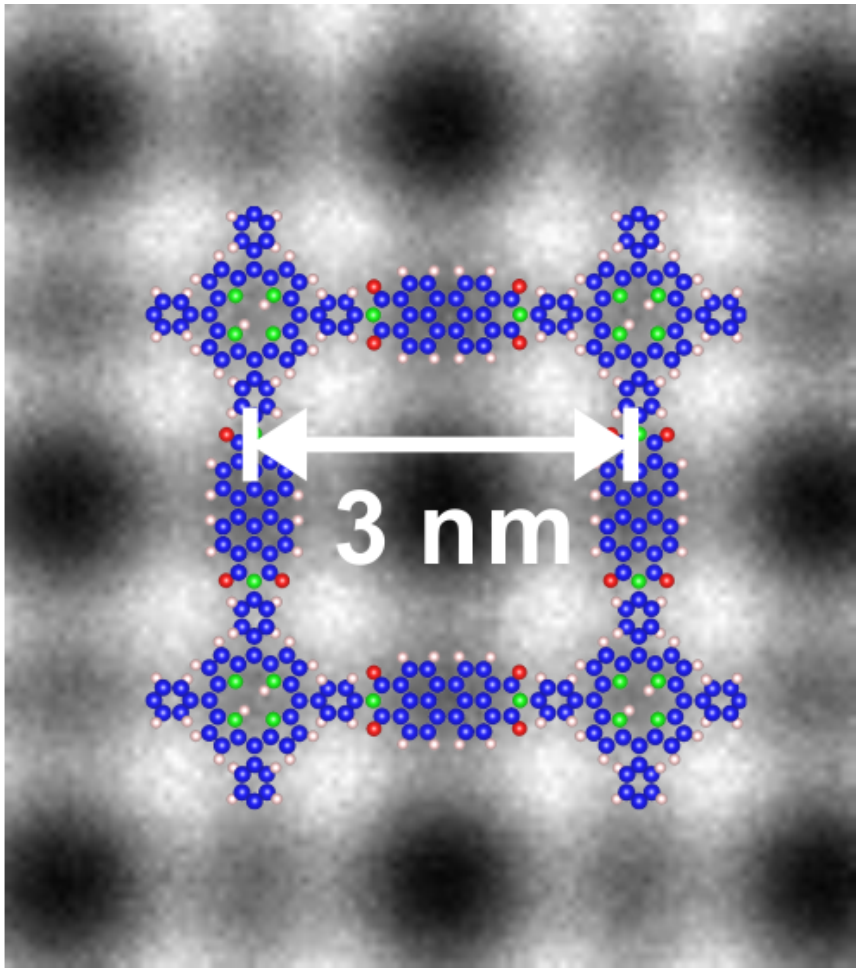
3 nm